ASM Sc. J., 18, 2023

https://doi.org/10.32802/asmscj.2023.1290

# The Strong Effect of Fe on the Structural and Optical Properties of $CdTiO_3$

R. Bahloul* and S. Sayouri

*LPAIS Department of Physics, Faculty of Science DM, USMBA, BP 1796, Fez-Atlas, Fez, 30000, Morocco*

Fe-doped Cadmium titanium oxide ($CdTiO_3$) powders were prepared by the sol-gel method. The samples were characterised by Fourier-transform infrared (FTIR) spectroscopy, Electron paramagnetic resonance (EPR) technique, x-ray diffraction (XRD) and diffuse reflection spectroscopy (DRS). The X-ray diffraction results show well that all the samples displayed the ilmenite structure with the presence of minor traces of Titanium Dioxide ($TiO_2$) and (Cadmium oxide) CdO phases, which ratio was shown to change with various concentrations in Fe. The estimated average particle size of the samples was around 56 nm. The photoluminescence properties of Fe-doped $CdTiO_3$ were investigated. FTIR spectroscopy showed the presence of the Ti-O and CdO vibration bands. The spectra from the diffuse reflectance spectroscopy (DRS) DRS showed a red shift and a strong reduction of the gap energy compared to that of the pure sample ($CdTiO_3$). The crystal structure of the $CdTiO_3$ nano-powder presented a certain level of distortion due to the high concentration of oxygen vacancies. In fact, under (400) nm excitation, a clear green emission consecutive to oxygen vacancies was observed. The luminescence spectra of the Fe- doped $CdTiO_3$ samples revealed that, due to oxygen vacancies, the emission and absorption intensities were both enhanced when the size was decreased. It can be inferred from our studies that the concentration of oxygen vacancies could be increased by reducing the crystallite size. The optical and ESR studies showed that the form of bivalent and trivalent states of iron were observed in distorted octahedral symmetry.

**Keywords:** Fe-doped $CdTiO_3$; Diffuse reflectance; band gap; EPR; photoluminescence

## I. INTRODUCTION

$CdTiO_3$ nanopowders exhibit several physicochemical properties that make them suitable for different applications, such as in materials science and in electronic field, which are strongly dependent on different parameters such as morphology, crystallite size and crystalline structure (Bahloul *et. al.,* 2017; Kharkwal *et. al.,* 2012; Montenero *et. al.,* 1997; Zhang *et al.,* 2003). Doping $CdTiO_3$ with elements belonging to the transition metals family, such as $Zn^{2+}$, $Ni^{2+}$, $Fe^{3+}$ or $Fe^{2+}$ has been shown to enlarge the absorption spectrum to the visible region, which may inhibit electron-hole recombination process (Choi *et. al.,* 1994; Epifani *et al.,* 2000). Great interest has been devoted to doping $CdTiO_3$ with $Fe^{3+}/Fe^{2+}$ due to their ionic radius (R($Fe^{3+}$) = 0.64/R($Fe^{2+}$) = 0.78 Å) comparable to that of $Ti^{4+}$ (0.68 Å) but not to that of $Cd^{2+}$(0,99 Å). Therefore, Fe ion can be easily incorporated into the $TiO_6$ and $CdO_6$ octahedra (Bahloul *et al.,* 2018). The band gap energy of $TiO_2$ is 3 eV for rutile and the band gap of cadmium oxide is in the range of 2.2 - 2.7 eV (Tawfik *et al.,* 2017), which will reduce the width of the energy gap of Fe-doped $CdTiO_3$ and increase the efficiency of absorbing visible light.

Several techniques are usually employed to elaborate Fe-doped $CdTiO_3$, Zhang et al. (Zhang *et al.,* 2003) prepared a $CdTiO_3$ powder by a sol–gel hydrothermal method at 200°c using cadmium acetate and tetrabutyl titanate. Wang *et al.* (2002) prepared a pure single phase of $CdTiO_3$ with hexagonal structure at 120°C by a hydrothermal route. The controlled hydrolysis, co-precipitation, and sol-gel

*Corresponding author's e-mail: radouane.bahloul1270809@gmail.com

techniques are largely adopted because of its simplicity, and its comparatively lower synthesis temperature (Zhu *et. al.,* 2004; Yang *et al.,* 2017). Cadmium titanium ($CdTiO_3$) is another type of $ABO_3$ Ilmenite, which has a large optical response and which properties and consequently its field of applications can be improved when doped with magnetic ions. The present work aims to study the influence of Fe doping on the structural and optical properties of $Cd_{(1-x)}FexTiO_3$ solid solutions with x=0.01, 0,025, 0.05 and 0.1. our main motivation in conducting the study is to further understand the physical properties of the elements. This will contribute to more informed and efficient application of the results in industrial and technological fields.

## II. EXPERIMENTAL SECTION

The sol-gel process was used to prepare the Fe-doped $CdTiO_3$ samples (Bahloul *et al.,* 2017). First, 10 mL of titanium tetraisopropoxide was dissolved in 100 mL of ethanol and then the water solution of iron acetate was used to obtain different concentrations in Fe in $CdTiO_3$: 1 %, 2.5 %, 5 %, and 10 %. Some drops of acetic acid were then added. The obtained solution was then stirred at room temperature for 10 min (Bahloul *et al.,* 2017). A calcination of the product was performed The powders were calcined for 2hrs at 900°C to obtain Fe-doped $CdTiO_3$ nanopowders. The physical properties of the samples were characterised with the help of different techniques. XRD analysis was carried out with 2θ in the range of 10-90° using an X-Pert Professional diffractometer apparatus with Cu-Ka (k = 1.5406 Å) radiation. FTIR spectroscopy was used to determine the stretching bond and functional groups with the help of a Spectrum RX instrument. (DRS) allowed us to determine the band gap energy of the samples. All characterisations were carried out at room temperature.

## III. RESULTS AND DISCUSSION

### *A. Structure Analysis*

The phase composition and crystalline structure of Fe-doped $CdTiO_3$ nanopowders at different doping concentrations were characterised using XRD. As shown in Figure 1, the XRD patterns of the annealed samples are of Ilmenite structure with R-3 space group and trigonal symmetry (JCPDS Card No. 029-0277) (Bahloul *et al.,* 2017). All the diffractograms showed the Ilmenite structure of the Fe-doped $CdTiO_3$ samples with the presence of secondary phases ($TIO_2$ rutile/CDO mixed), confirmed by the presence of their peaks in the XRD patterns (+, $TiO_2$; °, CdO).

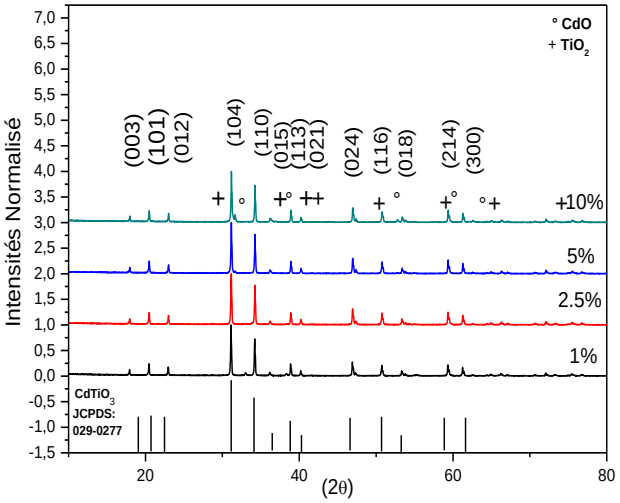


Figure 1. X-ray diffraction patterns of the Cd(1-x)FexTiO$_3$ powders

Indeed, the observed peaks of the Fe-doped $CdTiO_3$ phase at the angles of 17.9194, 20.4495, 22.9452, 34.1847, 36.1218, 38.8587, 46.8976, 50.7209, 53.3174, 59.2272, and 61.0214 (Figure 1) correspond to the (003), (101), (012), (104), (110), (015), (113), (021), (024), (116), (018), (214) and (300) planes, respectively. The proportion of the dominant peaks of $CdTiO_3$, $TiO_2$, and CdO phases for all the samples are shown in Table 1.

Table 1. The ratio of dominant $CdTiO_3$, $TiO_2$, and CdO phases for all samples

| Fe % | $CdTiO_3$ % | $TiO_2$ % | CdO % |
|---|---|---|---|
| 1 | 88 | 0 | 12 |
| 2.5 | 88 | 12 | 0 |
| 5 | 95 | 5 | 0 |
| 10 | 78 | 22 | 0 |

The values given in Table 1 show that the samples doping with Fe increased the secondary phases of $TiO_2$.

The crystallite size, D, of the samples was evaluated with the help of the following Debye–Scherrer's formula (Equation (1)):

$$D = \frac{0.9\lambda}{\beta COS\theta} \quad (1)$$

where λ is the wavelength of the X-ray used (λ= 1.5406 Å), β is the full width at half maximum (FWHM), θ is the angle between the incident ray and the scatter plane (Bragg angle). The average crystallite sizes of the samples appear in Table 2.

Table 2. Crystallite size and cell volume as functions of iron content

| X % | Crystallite size | A | C | Volume |
|---|---|---|---|---|
| 1 | 58.92983 | 5.23 | 14.84 | 351.42667 |
| 2.5 | 55.00518 | 5.23 | 14.8 | 350.47943 |
| 5 | 55.00652 | 5.23 | 14.78 | 350.00581 |
| 10 | 55.00785 | 5.23 | 14.76 | 349.53218 |

The crystallite size (CS) of the Fe-doped $CdTiO_3$ samples showed an abrupt decrease until x = 0.025 (Figure 2) and then remained practically constant pointing out that the limit of solubility of Fe in $CdTiO_3$ may be reached around this concentration; however, the observed slight increase in the CS for x > 0.025 may be due to an over aggregation of iron atoms in the $TiO_6/CdO_6$ octahedral site (Marami *et al.,* 2018). The variation of the lattice parameter, c, of the Fe-doped $CdTiO_3$ samples, which values are given in Table 2, is plotted in Figure 3. Due to the increase in the Fe content, the lattice parameter c, and, therefore, the volume of the unit cell, decreased (Figure 2) because of the difference between the ionic radii of $Cd^{2+}$(0,99 Å) and $Fe^{2+}$(0.78 Å) ions. Therefore, the distortion on the crystal structure of the doped samples could be related to the existence of oxygen vacancies in Fe-doped $CdTiO_3$ (Abazovic *et al.,* 2006). The occurrence of these oxygen vacancies has been evidenced from Raman and Photoluminescence analyses detailed below.

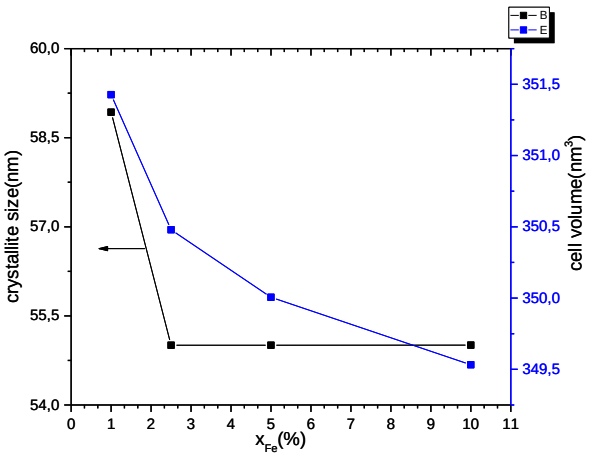


Figure 2. Variations of the crystallite size and cell volume with (X %) in Fe

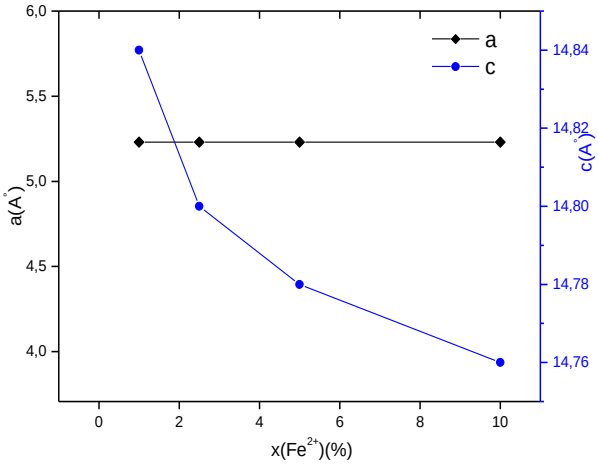


Figure 3. Variation of the lattice parameters with x % in Fe

### *B. Raman Analysis*

The Raman spectra of the as-prepared Fe-doped $CdTiO_3$ compounds for different compositions were recorded at room temperature, with the help of a Bruker's VERTEX 70v FT-IR Spectrometer and are displayed in Figure 4 in the wavenumber range of 100 - 900 $cm^{-1}$. The obtained Raman bands could be assigned to ilmenite modes (Bahloul *et al.,* 2017), which indicates that the structural evolution is in good accordance with X-ray diffraction results. Moreover, these recorded Raman modes agree well with those published elsewhere (Abazovic *et. al.,* 2008; Grasser & Scharmann, 1976). Figure 4 exhibits six broad bands centred at 218, 247, 330, 466, 600, and 700 $cm^{-1}$. The Ti-O vibration (Grasser & Scharmann, 1976; Min *et al.,* 1999) dominates the modes in the range 200 - 300 $cm^{-1}$.

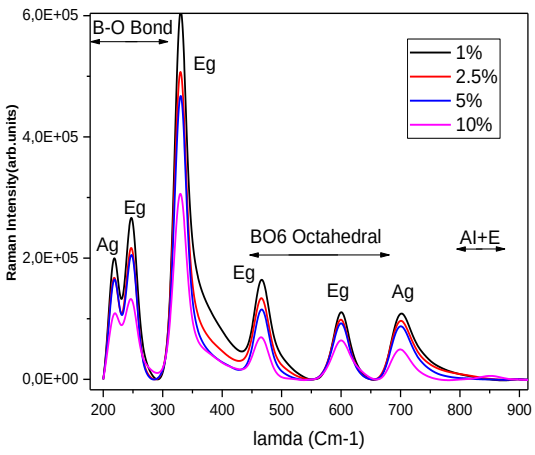


Figure 4. Raman spectra of $Cd_{(1-x)}FexTiO_3$ ceramics with different compositions

The modes centred at 600 - 700 $cm^{-1}$ are associated with the vibration of $TiO_6$ octahedra (Grasser & Scharmann, 1976; Min *et al.,* 1999). The latest mode (i.e., at 852 $cm^{-1}$) can be correlated to the presence of oxygen vacancies (Singha *et al.,* 2010).

The group theory calculation made by Rodrigues *et al.* (2018) showed that the rhombohedral structure belonging to the R-3 space group (C32i or #148) was adequate to describe the ilmenite system (ICSD card N° 262708) (The number of degrees of freedom for the ilmenite phase is 3n-6). As both Raman and infrared spectra at room temperature of $CdTiO_3$ are well documented in the literature (Bahloul *et al.,* 2017), therefore ten Raman active modes (5Ag ⊕ 5Eg) and eight infrared ones (4Au ⊕ 4Eu) are expected for $CdTiO_3$. To better understand the spectral evolution, we have carried out a deconvolution of the Fe-doped $CdTiO_3$ Raman spectra with Peakfit software using a [Gauss + Lor Amp] function, which leads to nine vibration modes as shown in Figure 5.

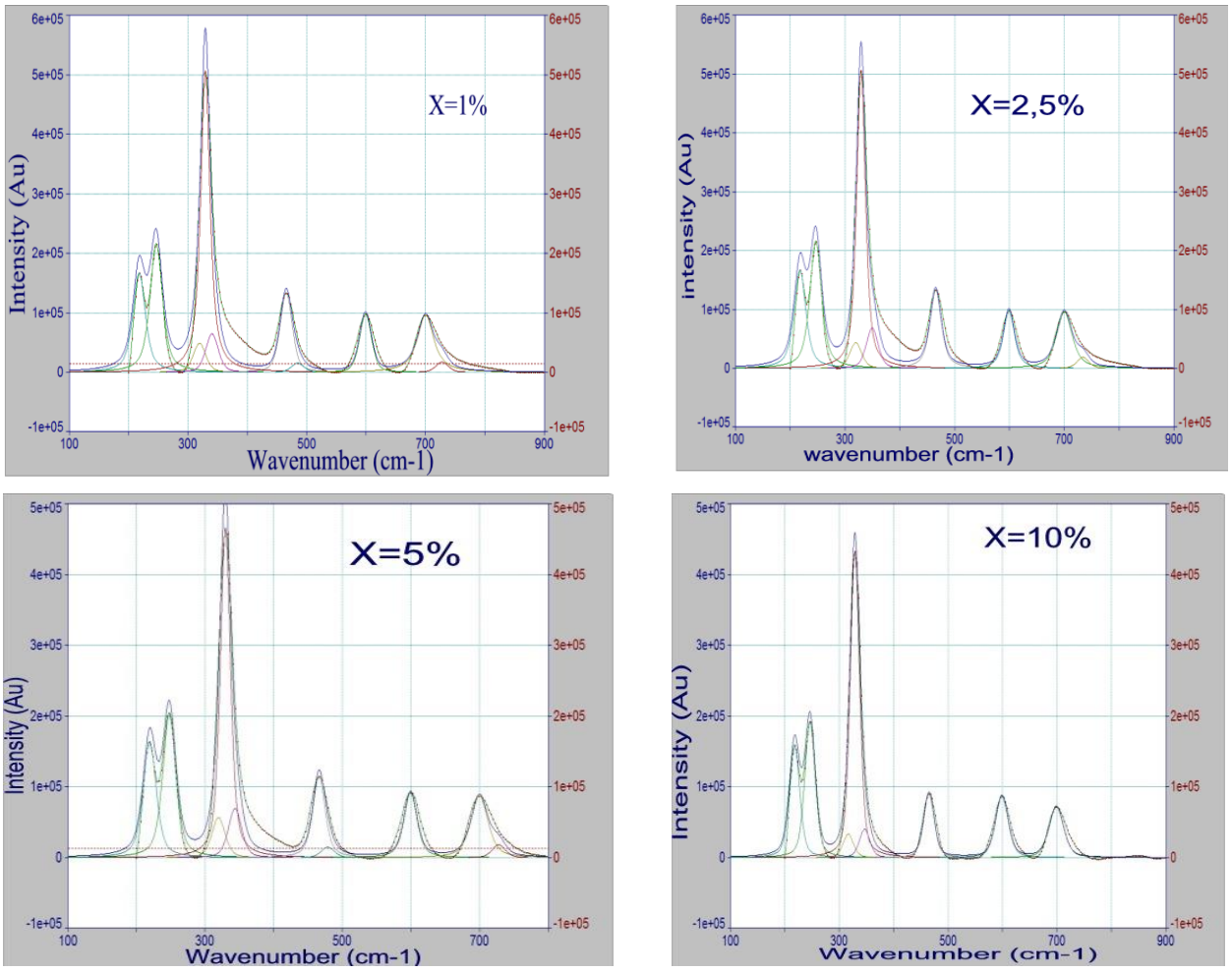


Figure 5. The deconvoluted Raman spectra of $Cd_{(1-x)}FexTiO_3$ ceramics with different compositions

For all samples, the first mode (i.e. at 230.5 $cm^{-1}$), is split into two modes (i.e. at 217 and 247 $cm^{-1}$). The high intensity of this peak is well observed from the composition of x = 5%. The broadband centred around 329 $cm^{-1}$ is split into three modes (i.e. at 320,329 and 354 $cm^{-1}$). For the third mode (i.e. at 466 $cm^{-1}$) and the fifth mode (i.e. at 700 $cm^{-1}$) are split into two modes as shown in Figure 5.

The overall evolution of the position frequency and full width at half maximum (FWHM) of individual peaks are plotted in Figure 6. It can be easily seen that a drastic change occurs between 5 % and 10 % in Fe. The first mode (i.e. at 218 $cm^{-1}$) displays a shift to the higher frequencies as the composition (x) increases (up to about 218.9 $cm^{-1}$ for x = 0.05). The broad band centred around 330 $cm^{-1}$ splitted into three modes (i.e., 320.12, 330.24 and 356.16 $cm^{-1}$ for 1%); this is also true for all the samples. We also observed that the position and FWHM of all the modes show a similar type of anomaly at x = 0.05. On the basis of these considerations, it is possible to conclude that the rhombohedral phase of $CdTiO_3$ and the secondary phase of $TiO_2$ coexist at x = 0.05 - 0.1, which was also evidenced in the XRD results.

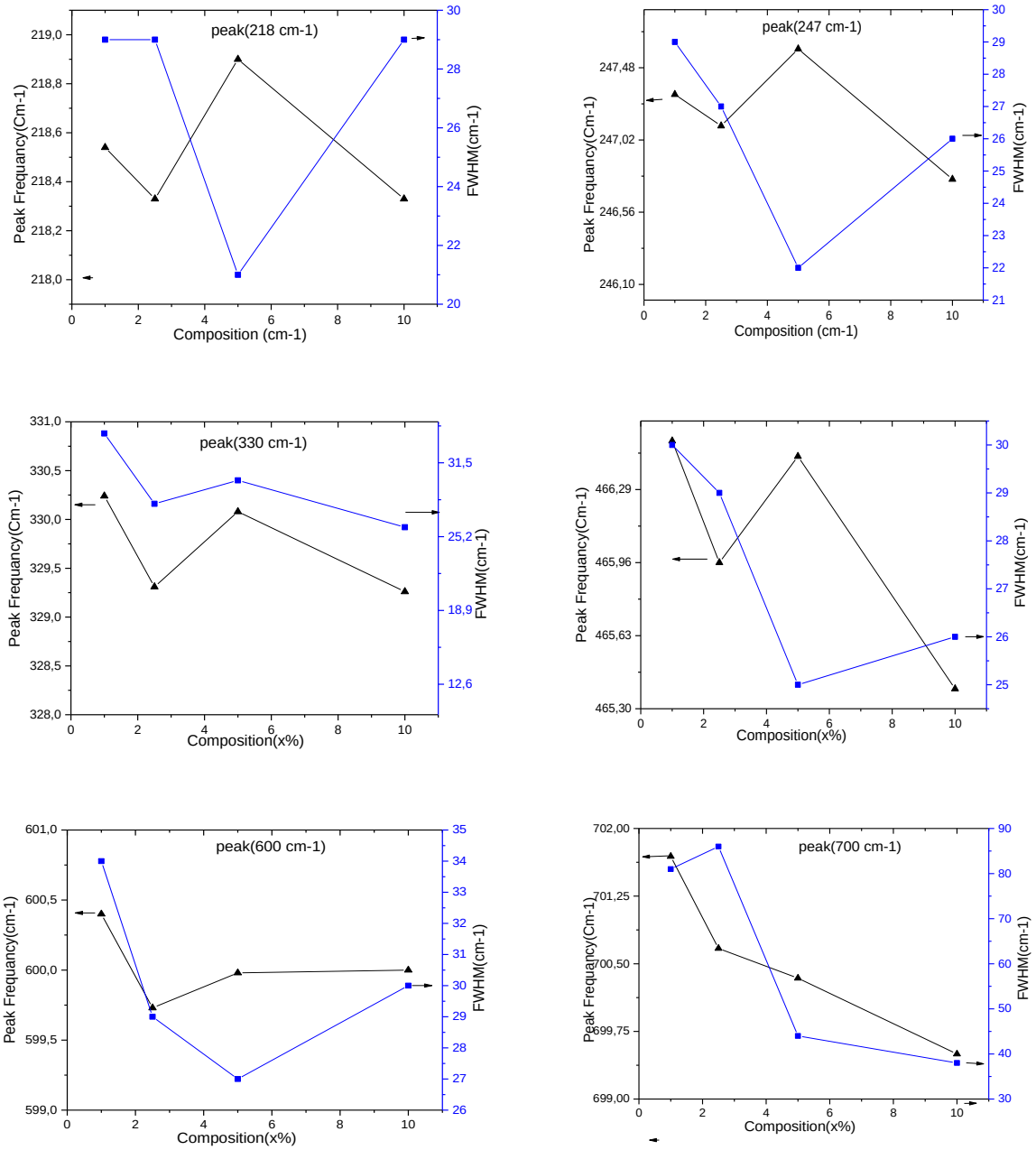


Figure 6. Variations of the peak positions and FWHM of different modes in the Raman spectra

Figure 7 shows the rhombohedral structure which represents the atoms of ilmenite phase: the cations A ($Cd^{2+}/Fe^{3+}$) as well as the cations B ($Ti^{4+}$) are not situated at the centre of the octahedral cavity thus suggesting a cationic displacement. The theoretical Goldschmidt factor (t = 0.82) explains the phase distortion of the system. Given that t < 1, it is therefore probable that this observed local disorder is due to the difference between $Cd^{2+}$ ionic radius ($RCd^{2+}$ = 0.99 Å) and that of Fe ($RFe^{3+}$ = 0.64, $RFe^{2+}$= 0.76 Å) causing distortions of [$CdO_6$] and [$TiO_6$] octahedra.

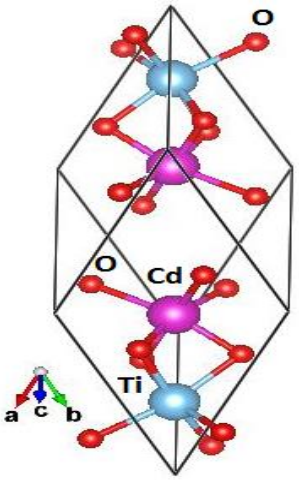


Figure 7. $CdTiO_3$ crystal with rhombohedral structure

### *C. FTIR Spectroscopy*

FTIR analysis allowed the determination of the vibration bands of the samples in the range of 400 to 4000 cm-1 wave numbers. The corresponding spectra of the Fe-doped $CdTiO_3$ samples, as shown in Figure 8. The band around 2900 $cm^{-1}$ can be ascribed to the symmetrical stretching vibration of the C=C bond. The stretching vibration of the $CO_2$ bond causes the peak at 2317 $cm^{-1}$, and the weak peaks at 1740 $cm^{-1}$ and 1498 $cm^{-1}$ are due to the bending vibration of O–H and C–H groups, respectively.

Finally, the metal-oxygen length (Ti–O/Cd–O) group may cause the strong absorption peak located in the range of 470 and 670 $cm^{-1}$. It can also be noticed that increasing Fe content gave rise to the decrease in the amount of the transmittance intensity. The latter increased until 2.5% in Fe but decreased above this concentration until 10%. The increase of transmittance is due to the electrons present in the 3d6 level of iron (Marami *et al.,* 2018), and the increased absorption is due to the increasing of the number of electrons by adding impurity to 10% (Marami *et al.,* 2018).

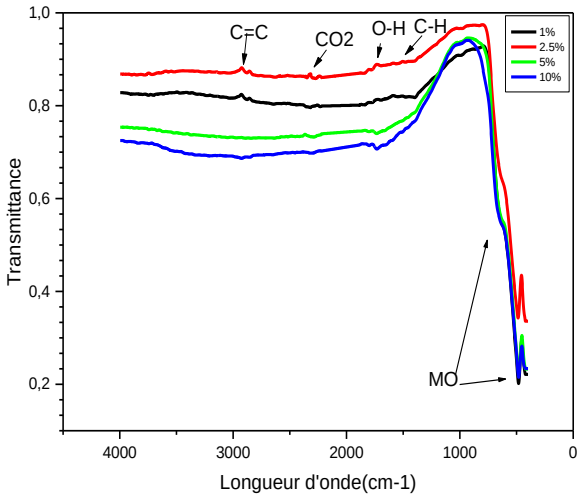


Figure 8. FTIR spectra of Fe-doped $CdTiO_3$

### *D. UV-Vis DRS Analysis*

UV–vis diffuse reflectance spectroscopy (DRS) spectra were recorded in the wavelength range of 250 to 800 nm for the pure and Fe-doped $CdTiO_3$ at different concentrations. The direct band gap was estimated from the reflectance spectra by extrapolating the linear portion of the [F(R)*hv]2 versus Eg plot to F(R) = 0; the band gap energy is given by the intercept value, as shown in Figure 9. The direct band gap energy (Eg) of the Fe-doped $CdTiO_3$ was estimated from the UV-DRS measurements using the Kubelka–Munk function Equation (2), and the F(R) value was calculated from the following equation:

$$F(R) = \frac{K}{S} = \frac{(1-R)^2}{2R} = \alpha \quad (2a)$$

and

$$\alpha.hv = A(hv-Eg)1/2 \quad (2b)$$

Where F(R) is the Kubelka–Munk function and R is the percentage reflectance. Figure 10 shows the variation of the optical band gap energy (Eg) as a function of the iron concentration. It is observed a decrease in the UV region of the reflectance intensity with the increase in impurities. Indeed, a strong reduction of Eg of the pure sample ($CdTiO_3$; Eg = 3.86 eV (Bahloul *et al.,* 2017)) is observed under doping with 1% in Fe (Eg = 1.76 eV). After an increase of Eg (= 1.81 eV) for the sample with x = 5%, another drop of Eg (= 1.6 eV)

is recorded under doping with 10% in Fe ions, pointing the role played by the disorder introduced by Fe in the $CdTiO_3$ matrix. The reduction in the band gap energy causes the absorbance peak to shift toward longer wavelengths known as a redshift. In comparison with previous literature, the effect of iron on the energy gap in the $CdTiO_3$ compound is larger than that of Ni and Zn (Kharkwal *et al.,* 2012).

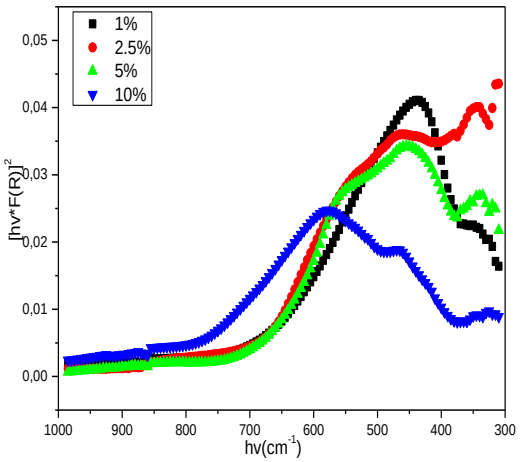


Figure 9. Direct band gap energy of $Cd_{(1-x)}FexTiO_3$ calcined at 900°C

It is known that the reduction of the band gap under doping - the introduction of impurities into an intrinsic semiconductor introduces intermediate levels in the band gap of the samples - is due to different parameters, such as structure distortion, change in lattice parameters, particle size (Marami *et al.,* 2018). These results are in conformity with the XRD analysis, where the particle size changes with incorporation of iron. It can be noticed that the lowest crystallite size and band gap values were observed for 10 % in Fe (Figure 10).

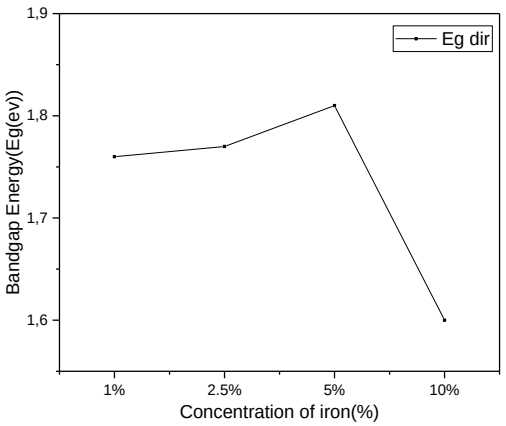


Figure 10. Variation of the optical band gap energy with iron content in $Cd_{(1-x)}FexTiO_3$

### *E. Photoluminescence (PL) Study*

Photoluminescence measurements were performed to investigate the influence of the particle size on the photoluminescence (PL). Figure 11 shows the PL emission spectra of Fe-doped $CdTiO_3$ nanopowders excited at 280 nm. In the UV spectrum region, a decrease of the intensity of the peaks is observed for the two concentrations of 5 % and 10 % in Fe; for additional Fe impurity, this trend is reversed. In the visible region, the intensity of the peaks increased with Fe-doping except for the two concentrations 1 % and 2.5 %; the intensity of the latter is lower than that of 1 %.

The high-energy peaks could be the result of band edge luminescence of the $CdTiO_3$, while lower energy peaks are induced by the presence of oxygen vacancies (Marami *et. al.,* 2018; Abazovic *et. al.,* 2006; Abazovic *et al.,* 2008). The predominant emission band centred around 450 nm could be ascribed to the electronic transition from Fe 5d state to oxygen 2p state, so in Fe-doped $CdTiO_3$ structure, $Cd^{2+}$, $Ti^{4+}$ and $Fe^{2+}$ ions occupy the octahedral sites [XO6] (X = $Cd^{2+}$, $Ti^{4+}$, $Fe^{2+}$), in which electrons could be transferred between $O^{2-}$ to $Xn^{+}$ ions giving rise to the characteristic absorption and emission of $CdTiO_3$ (Bahloul *et. al.,* 2018; Grasser & Scharmann, 1976; Min *et al.,* 1999). As shown in Figure 11, the relative emission intensity of the samples increased as the particle size decreased. However, more defects could be generated in smaller nanopowder samples causing the emission intensity to increase (Jia *et al.,* 2012).

The broadening (inset, Figure 11) of PL spectra and emission intensity of oxygen vacancies show an increasing trend with iron concentration. That is may be due to the

concentration of oxygen vacancies in Fe-doped $CdTiO_3$ nanopowders, which increased with a decrease in particle size (Bahloul *et al.,* 2018).

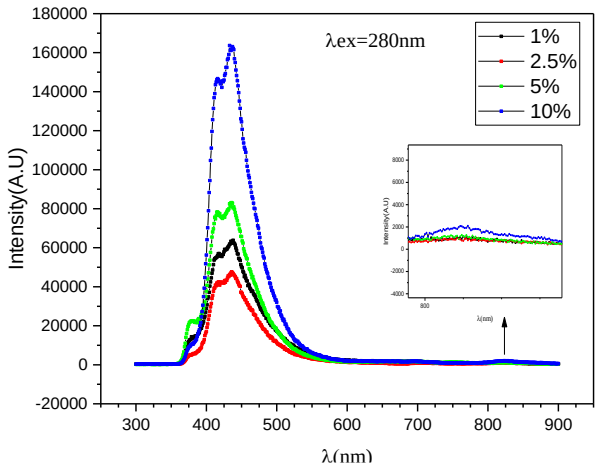


Figure 11. PL spectra of 1 %, 2.5 %, 5 %, and 10 % nanopowder excited by 270 nm

### *F. EPR Studies*

The EPR spectra were recorded, at room temperature, on an EPR spectrometer in the X-band frequency (≈ 9.400 GHz). The Fe-doped $CdTiO_3$ samples showed resonance signals; Figure 12 shows typical EPR spectra for $Fe^{3+}$, $Fe^{2+}$, and $Ti^{3+}$ ions with concentrations such as 1 %, 2.5 %, 5 % and 10 %. When Fe content is ≤ 5%, the EPR spectra mainly consist of an intense resonance signal at g ≈ 2.04 attributed to $Fe^{3+}$ (Singha *et al.,* 2010), the others resonance signals at g = 1.97 and g = 1.83 - 2.36 are ascribed to $Ti^{3+}$ and $Fe^{2+}$, respectively. When Fe content is equal to 0.1, the EPR spectrum shows a disappearance of all shoulders except that corresponding to g ≈ 2.04 signal.

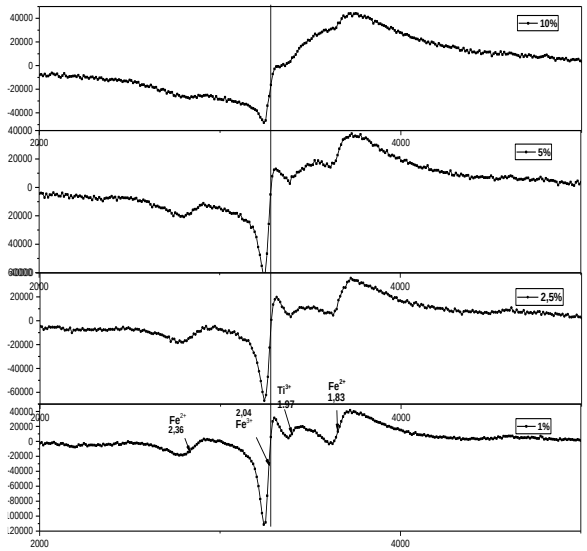


Figure 12. EPR spectra of ions (x=1 %, 2.5 %, 5 %, and 10 %)

It can be noticed that isotropic g values arise when certain symmetry elements in samples are present and related to the coordination number (Nofz *et. al.,* 1990; Rodrigues *et al.,* 2018). The absorption at g ≈ 2.04 arises from $Fe^{3+}$ ions in octahedral coordination. In the present study, the EPR spectra for all concentrations mainly consisted in an intense resonance signal at g ≈ 2.04, which is attributed to the isolated Fe3+ ions predominantly situated in a distorted rhombohedral environment (Bahloul *et al.,* 2018). From the observed g values, as shown in Figure 12, it is clear that the iron ions also exist in their trivalent state and the corresponding site of symmetry is a distorted octahedron.

## IV. CONCLUSION

The Fe-doped $CdTiO_3$ nanopowders, with an average particle size of around between 54 to 58 nm, were successfully prepared by the sol-gel method. The structure of the samples was determined to be ilmenite with a rhombohedral phase, with the presence of a minority of secondary phases ($CdO/TiO_2$). The XRD results also revealed that the crystallite size decreased with an increase of Fe content, and this parameter reached its minimum value of about 55 nm for 10% in Fe.

A vibration of the M-O (M = Cd, Ti) bond in the range of 528 - 458 $cm^{-1}$ could be seen from FTIR analysis. The lattice modes for 5% were found to exhibit anomalies in their intensity and linewidth. The PL spectra decreased in the intensity for the UV and visible regions. The UV-DRS results

showed a red shift due to the reduction of the band gap caused by the increase of Fe content. The EPR spectra of $Fe^{2+}$ ions exhibited two resonance signals at g ≈ 1.83, g ≈ 2.36, g = 1.97 for $Ti^{3+}$ and g = 2.04 for $Fe^{3+}$ which are in rhombohedral sites. The electron spin resonance and optical studies confirmed that iron ions may also be present in their trivalent state in a distorted octahedral environment. The photoluminescence spectra suggest that the emission and absorption of Fe-doped $CdTiO_3$ nanopowders that appeared as a consequence of oxygen vacancies were both enhanced with a decreasing of particle size.

The above obtained results in Fe-doped $CdTiO_3$ ilmenite structure with different particle sizes would be helpful for further research and application of Fe-doped $CdTiO_3$ nanopowders. Moreover, the effect of Fe ions, in terms of disorder and defects, on the above described physical properties are more stronger than that of Ni or Zn ones.

## V. ACKNOWLEDGEMENT

One of us (R.B.) is thankful to Dr. Boujemaa Jaber responsible for UATRS division at the National Center for Scientific and Technical Research (CNRST), for providing experimental results and helpful discussions.

## VI. REFERENCES

Abazovic, ND, Comor, MI, Dramicanin, MD, Jovanovic, DJ, Ahrenkiel, SP & Nedeljkovic, JM 2006, 'Photoluminescence of Anatase and Rutile $TiO_2$ Particles', Phys. Chem., B, vol. 110, no. 50, pp. 25366–25370.

Abazovic, ND, Ruvarac-Bugarcic, IA, Comor, MI, Bibic, N, Ahrenkiel, SP & Nedeljkovic, JM 2008, 'Photon energy up-conversion in colloidal $TiO_2$ nanorods', Opt. Mater., vol 30, no. 7, pp. 1139-1144.

Ali, T, Tripathi, P, Azam, A, Raza, W, Ahmed, AS, Ahmed, A & Muneer, M 2017, 'Photocatalytic performance of Fe-doped $TiO_2$ nanoparticles under visible-light irradiation', Mater. Res. Express, vol. 4, no. 1, pp. 015022.

Asahi, R, Morikawa, T, Ohwaki, T, Aoki, K & Taga Y 2011, 'Visible-light photocatalysis in nitrogen-doped titanium oxides', Science, vol. 293, pp. 269-271.

Bahloul, R, Karoum, L, Hamzah, M, Khenfouch, M, Srinivasu, VV & Sayouri, S 2018, 'Optical and magnetic properties of $Cd_{(1-x)}FexTiO_3$ (x = 1%)', Materials Science: Materials in Electronics, vol. 29, no. 23, pp. 19854–19860.

Bahloul, R, Sayouri, S, Limame, K, Mustapha Yahyaoui, M, Jaber, B & Laanab, L 2017, 'Temperature effect on the structural and the optical properties of sol gel $CdTiO_3$ Nanopowders', Ceramic Processing Research, vol. 18, no. 4, pp. 329-335.

Choi, J, Park, H & Hoffmann M 2010, 'Effects of Single Metal-Ion Doping on the Visible-Light Photoreactivity of $TiO_2$', Chem. Vol. 114, no. 2, pp. 783–792.

Choi, WY, Termin, A & Hoffmann, MR 1994, 'The Role of Metal Ion Dopants in Quantum-Sized TiO2: Correlation between Photoreactivity and Charge Carrier Recombination Dynamics', Phys. Chem., vol. 98, no. 51, pp. 13669–13679.

Epifani, M, Giannini, C, Tapfer, L & Vasanelli, L 2000, 'Sol–Gel Synthesis and Characterization of Ag and Au Nanoparticles in $SiO_2$, $TiO_2$, and $ZrO_2$ Thin Films', Am. Ceram. Soc., vol. 83, no. 10, pp. 2385-2393.

Grasser, R & Scharmann, A 1976, 'Luminescent sites in $CaWO_4$ and $CaWO_4$: Pb crystals., Lumin, vol. 12, no. 13, pp. 473-478.

Hiran, M, Joji, T, Inagaki, M & Iwata, H 2004, 'Direct Formation of Iron (III)-Doped Titanium Oxide (Anatase) by Thermal Hydrolysis and Its Structural Property', Am. Ceram. Soc., vol. 87, no. 1, pp. 35-41.

Izmajlowicz, MAT, Flewitt, AJ, Milne, WI & Morrison, NA 2003, 'Directional nickel-induced fielded aided lateral crystallization of amorphous silicon', Journal of Applied Physics, vol. 94, no. 12, pp. 7535-7541.

Jia, Y, Qiao, H, Zheng, Y, Guoab, N & You, H 2012, 'Synthesis and photoluminescence properties of $Ce^{3+}$ and $Eu^{2+}$ -activated $Ca_7Mg(SiO_4)_4$ phosphors for solid state lighting', Physical Chemistry Chemical Physics, vol. 14, no. 10, pp. 3537-3542.

Kachina, A, Puzenat, E, Ould-Chikh, S, Geantet, C, Delichere, P & Afanasiev, P 2012, 'A New Approach to the Preparation of Nitrogen-Doped Titania Visible Light Photocatalyst', Chem. Mater, vol. 24, no. 4, pp. 636–642.

Kharkwal, M, Uma, S & Nagarajan, R 2012, 'Synthesis and optical properties of pure $CdTiO_3$ and $Ni^{2+}$ and $Zn^{2+}$ ion

substituted $CdTiO_3$ obtained by a novel precursor route', Indian and Journal of Chemistry, vol. 51, no. 11, pp. 1538-1544.

Liu, H, Wu, Y & Zhang J, 2011, 'A new approach toward carbon-modified vanadium-doped titanium dioxide photocatalysts and A.C.S. Appl', Mater. Interfaces, vol. 3, no. 5, pp. 1757–1764.

Liu, S, Liu, X, Chen, Y & Jiang, R 2010, 'A novel preparation of highly active iron-doped titania photocatalysts with a p–n junction semiconductor structure', Alloys Compd., vol. 506, no. 2, pp. 877-882.

Marami, MB, Farahmandjou, M & Koshnevisan, B 2018, 'Sol-Gel Synthesis of Fe-Doped $TiO_2$ Nanocrystals', Electronic Materials, vol. 47, no. 7, pp. w3741–3748.

Min, K, Mho, WS & Yeo, IH 1999, 'Electrochemical Fabrication of Luminescent $CaWO_4$ and $CaWO_4$: Pb Films on W Substrates with Anodic Potential Pulses', Electrochem. Soc., vol. 146, no. 8, pp. 3128-3136.

Montenero, A, Canali, M, Gnappi, G, Bersani, D, Lottici, PP, Nunziante, P & Traversa, E 1997, 'Structural and electrical-properties of sol-gel-processed $CdTiO_3$ powders and films', Applied Organometallic Chemistry, vol. 11, no. 2, pp. 137-146.

Nofz, M, Stosser, R & Wihsmann FG 1990, 'Paramagnetic centres in glasses of the system $CaO$-$Al_2O_3$-$SiO_2$', Phys. Chem. Glasses, vol. 31, no. 2, pp. 57-63.

Pulsipher, DJV, Martin, IT & Fisher ER 2010, 'Controlled Nitrogen Doping and Film Colorimetrics in Porous $TiO_2$ Materials Using Plasma Processing', ACS Appl. Mater. Interfaces, vol. 2, no. 6, pp. 1743–1753.

Reginaldo, S, Santos, S, Guilherme, A, Carlos, AP Leite, S, Herbert, S, Marco, AZ & Longo, C 2012, 'Iron Insertion and Hematite Segregation on Fe-Doped $TiO_2$ Nanoparticles Obtained from Sol–Gel and Hydrothermal Methods and A.C.S. Appl', Mater. Interfaces, vol. 4, no. 10, pp. 5555–5561.

Rodrigues, JE, Ferrer, MM, Cunha, TR, Costa, RC, Sambrano, JR, Rodrigues, AD & Pizani, PS 2018, 'First-principles calculations and Raman scattering evidence for local symmetry lowering in rhombohedral ilmenite: temperature - and pressure-dependent studies', J. Phys.: Condens. Matter, vol. 30, no. 48, pp. 485401.

Singha, SP, Chakradhara, RPS, Raob, JL & Karmakara, B 2010, EPR, FTIR, 'Optical absorption and photoluminescence studies of $Fe_2O_3$ and $CeO_2$ doped ZnO–$Bi2O_3$–$B2O_3$ glasses', Journal of Alloys and Compounds, vol. 493, pp. 256–262.

Tawfik, WZ, Esmat, M & El-Dek, SI 2017, 'Drastic improvement in magnetization of CdO nanoparticles by Fe doping', Appl. Nanosci., vol. 7, pp. 863–870.

Wang, CY, Bottcher, C, 'Bahnemann DW & Dohrmann, JK 2003, 'A comparative study of nanometer sized Fe(iii)-doped $TiO_2$ photocatalysts: synthesis, characterization and activity', Mater. Chem., vol. 13, no. 9, pp. 2322-2329.

Wanga, H, Zhang, XX, Huang, AP, Xu, HY, Zhu, MK, Wang BO 2002, J. Cryst. Growth, vol. 246, 150.

Yang, Y, Yu, T, Wang, J, Zheng, W & Cao, Y 2017, 'Doping and transformation mechanisms of $Fe^{3+}$ ions in Fe-doped $TiO_2$', Cryst. Eng. Comm., vol. 19, no. 7, pp. 1100-1105.

Zhang, J, Pan, C, Fang, P, Wei, J & Xiong, R 2010, 'Mo + C codoped $TiO_2$ using thermal oxidation for enhancing photocatalytic activity', A.C.S. Appl, Mater. Interfaces, vol. 2, no. 4, pp. 1173–1176.

Zhang, X, Wang, H, Huang, A, Xu H, Zhang, Y, Yu, D 2003, J. Mater. Sci., vol. 38, 2353.

Zhang, X, Wang, H, Huang, A, Xu, H, Zhang, Y, Yu, D, Wang, B & Yan, H 2003, 'Synthesis of cadmium titanate powders by a sol-gel-hydrothermal method', Materials Science, vol. 38, pp. 2353-2356.

Zhang, X, Zhou, M & Lei, L 2006, 'Co-deposition of photocatalytic Fe doped $TiO_2$ coatings by MOCVD', Catal. Commun., vol. 7, no. 7, pp. 427-431,

Zhu, J, Zheng, W, He, B, Zhang, J & Anpo M 2004, 'Characterization of Fe–$TiO_2$ Photocatalysts Synthesized by Hydrothermal Method and Their Photocatalytic Reactivity for Photodegradation of XRG Dye Diluted in Water', J. Mol. Catal, vol. 216, no. 1, pp. 35-43.